CAMBRIDGE
UNIVERSITY PRESS

Article

Evidence of the anthropogenic origin of the 'Carmel sapphire' with enigmatic super-reduced minerals

Evgeny Galuskin (ID) and Irina Galuskina (ID)

Faculty of Natural Sciences, Institute of Earth Sciences, University of Silesia, Poland

Abstract

Corundum with inclusions of enigmatic super-reduced minerals was found in mineral separates received as a result of alluvial sediment exploration near Mt Carmel, Israel by the *Shefa Yamim* Company. This corundum, registered as 'Carmel sapphire^{TM}', has been an object of numerous publications by W. Griffin's scientific team, in which they propose a questionable hypothesis of sapphire formation at the crust–mantle boundary with the participation of CH_4+H_2 fluids. Typically the Carmel sapphire is in small fragments of breccia with white cement, which in the opinion of Griffin *et al.* is a carbonate-cemented volcanic ash. Our investigation of the 'white breccia' showed that it consists of unsorted angular fragments of Carmel sapphire from ~1 μm to 7 mm in size cemented by aluminium hydroxides (bauxite) and is a waste product of the fused alumina process, i.e. it has an anthropogenic origin. Phases typical for slags of fused alumina production and metallurgical slags were identified in the 'white breccia'. Carmel sapphire has numerous microscopic spherical inclusions of Si–Fe alloy indicating that the removal of Si and Fe from the corundum melt occurred at a temperature >2000°C. Osbornite, TiN, from Carmel sapphire has a chemical zonation characteristic of osbornite from fused alumina with enrichment of central zones in carbon. Comparison of the growth heterogeneity of Carmel sapphire and 'electrocorundum' indicates that the crystallisation of the corundum melt proceeded in a similar way. Unfortunately, in the case of Carmel sapphire from the Carmel locality, the contamination of geological samples with anthropogenic material has led to popularisation of biased views.

Introduction

In 2019, in the pyrometamorphic Hatrurim Complex rocks in the Negev Desert, Israel, we discovered a unique phosphide-bearing breccia, in which osbornite, TiN, was found *in situ* (Galuskin *et al.*, 2022; Fig. 1a,b; Fig. 2a,b). Osbornite is an indicator of the super-reduced conditions of rock genesis (Griffin *et al.* 2021a). It is a mineral typical of enstatite meteorites (Bannister, 1941; Weisberg *et al.*, 1988; Grokhovsky, 2006; Leitner *et al.*, 2018) and encountered extremely rarely on Earth. All 'terrestrial' findings of osbornite are associated exclusively with mineral separates of bulk geological samples (mineral fractions) (Tatarincev *et al.*, 1987; Dobrzhinetskaya *et al.*, 2009; Xu *et al.*, 2013; Xiong *et al.*, 2017, 2020, 2022; Griffin *et al.*, 2016a, 2016b, 2019a, 2021b; Silaev *et al.*, 2019; Yatsenko *et al.*, 2020, 2021). A skeletal osbornite occurring as inclusions in corundum from the alluvial sediments of Mt Carmel, North Israel, is the best known terrestrial osbornite (Griffin *et al.*, 2021a). Mineral separates (concentrates) mined by the *Shefa Yamim* Company (https://www.shefagems.com) as a result of exploration for gemstones in alluvial deposits are a source of this corundum. Osbornite in the corundum aggregates is associated with unusual super-reduced minerals

represented by nitrides, carbides, silicides, FeSi(±Ti,Cr,V)-alloys, and Ti^{3+}-bearing oxides (Griffin *et al.*, 2016b, 2018, 2019a,b, 2020a,b, 2021a,b; Bindi *et al.*, 2020).

This corundum with inclusions of super-reduced minerals obtained the trademark 'Carmel sapphire' and has been the host of 10 new mineral species discovered in the last five years and approved by the Commission on New Minerals, Nomenclature and Classification (CNMNC) of the International Mineralogical Association (IMA): carmeltazite (IMA2018-103) $ZrAl_2Ti_4O_{11}$ (Griffin *et al.*, 2018); kishonite (IMA2020-023) VH_2 (Bindi *et al.*, 2020); oreillyite (IMA 2020-030a) Cr_2N (Bindi *et al.*, 2020); griffinite (IMA 2021-110) Al_2TiO_5 (Ma *et al.*, 2022a); magnéliite (IMA2021-111) $Ti_2^{3+}Ti_2^{4+}O_7$ (Ma *et al.*, 2022b); ziroite (IMA2022-013) ZrO_2 (Ma *et al.*, 2022c); sassite (IMA2022-014) $Ti_2^{3+}Ti^{4+}O_5$ (Ma *et al.*, 2022d); mizraite-(Ce) (IMA2022-027) $Ce(Al_{11}Mg)O_{19}$ (Ma *et al.*, 2022e); toledoite (IMA2022-036) TiFeSi (Ma *et al.*, 2022f); and yeite (IMA2022-079) TiSi (Ma *et al.*, 2023). Grain aggregates of Carmel sapphire (and also hibonite and moissanite) from Carmel have been the objects of numerous scientific publications (Griffin *et al.*, 2016a,b, 2018, 2019a,b, 2020a,b, 2021a,b, 2022; Xiong *et al.*, 2017; Dobrzhinetskaya *et al.*, 2018; Cámara *et al.*, 2019; Bindi *et al.*, 2019, 2020; Huang *et al.*, 2020; Stan *et al.*, 2020; Oliveira *et al.*, 2021; Lu *et al.*, 2022), in which the authors present the highly controversial hypothesis that the corundum rock with super-reduced minerals formed at the crust–mantle boundary as a result of CH_4+H_2 fluid flowing through the magmatic melt.

Corresponding author: Evgeny Galuskin, Email: evgeny.galuskin@us.edu.pl; Irina Galuskina, Email: irina.galuskina@us.edu.pl

Figure 1. Localities of osbornite findings in Israel. (a) Negev Desert, Hatrurim Basin – the biggest area of the Hatrurim Complex pyrometamorphic rock outcrops in Israel. The location of (b) is shown in the frame. (b) Outcrop of low-temperature rocks of the Hatrurim Complex along the road Arad–Dead Sea, where phosphide-bearing breccia with osbornite was found (grey fragments of rock shown by arrow). A breccia fragment consisting of grey homogeneous clasts of the host rock cemented by gehlenite paralava is shown in the inset. (c) Typical view of re-cultivated fields after exploration of alluvial deposit by the *Shefa Yamim* Company. The numbers of the exploration drilling section based on the *Shefa Yamim* annual 2019 report are shown (Supplementary Fig. S1). (d) Current state of the Kishon River in the area of alluvial deposit exploration by the *Shefa Yamim* Company. All images were taken in 2022.

In the article "*Nitrogen under super-reducing conditions: Ti oxynitride melts in xenolithic corundum aggregates from Mt Carmel (N. Israel)*", Griffin *at al.* (2021b) described skeletal osbornite crystals, which are characterised by the variable composition forming solid solutions with TiC and TiO. The skeletal osbornite crystals are usually accompanied by an emulsion of osbornite, which the authors interpret as "*reflect*[*ing*] *the expulsion of N from the silicate melts during the eruption of the host magma*" (Griffin *et al.*, 2021b).

Recently, the natural origin of Carmel sapphire has been contested (Litasov *et al.*, 2019a; Ballhaus *et al.*, 2021), therefore comparing *in situ* osbornite from the Negev Desert with the skeletal osbornite crystals from the Carmel sapphire aggregates, and also with osbornite from 'electrocorundum' (fused alumina) became a prority. In 2022 we visited the Carmel locality at the Kishon River, Northern Israel (Fig. 1c,d). We succeeded in obtaining original material containing Carmel sapphire, which includes separated grains up to 100 μm in size, and also a small fragment ca. 7 mm, the so-called 'white breccia' with Carmel sapphire. Griffin *et al.* (2019b) describe 'white breccia' with Carmel sapphire as follows: "*The CS* [Carmel sapphire] *grains from the pyroclastic deposits, and even from the alluvial beds, commonly are coated in glass, but even more commonly by a fine-grained white breccia, consisting of carbonate-cemented volcanic ash. This cement is a result of eruption of the ashes on a shallow marine*

carbonate platform, and the subsequent covering of the ash beds by thick carbonate sequences." Griffin and co-authors (Griffin *et al.*, 2016b, 2018, 2019a,b, 2020a,b, 2021a,b) were not specific about the cement composition or corundum-free fragments of rock in the 'white breccia'. On only one occasion the amorphous carbon is recorded in the cement of the 'white breccia' (Xiong *et al.*, 2017).

In this paper we present a comparative study of osbornite from the Negev, Carmel and 'electrocorundum'. We present the results of a mineralogical study of the 'white breccia' with Carmel sapphire, which irrefutably indicate its anthropogenic origin. Our conclusions regarding the anthropogenic origin of Carmel sapphire are confirmed by the analysis of the growth inhomogeneity of Carmel sapphire and synthetic corundum using cathodoluminescence (CL).

An optical microscope, scanning electron microscopes Quanta 250/EDS and Philips XL30/EDS/CL, and Raman spectrometer WITec alpha 300R were the main equipment used to investigate the 'white breccia'. In this paper we use mineral names describing their synthetic analogues.

Israeli osbornite

Osbornite from the phosphide-bearing breccia of the pyrometamorphic Hatrurim Complex, found in the Negev Desert was
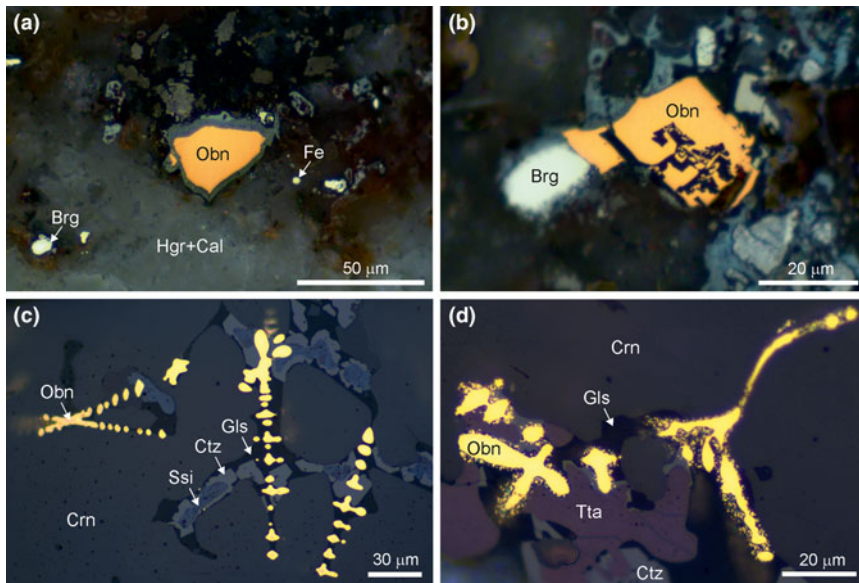
Figure 2. Morphology of osbornite found in Israel. (a, b) Osbornite in phosphide-bearing breccia of the Hatrurim Complex: (a) xenomorphic grain with rutile rim; and (b) crystal with morphological elements of skeletal growth. (c, d) Skeletal crystals in sapphire from Carmel confined to glass inclusions and associated with carmeltazite and Ti^{3+}-bearing oxides: (c) typical rounded surfaces of skeletal crystals formed from the melt; and (d) emulsion of osbornite near its skeletal crystals. Brg = barringerite, Cal = calcite, Crn = corundum, Ctz = carmeltazite, Fe = native iron, Gls = glass, Hgr = hydrogrossular, Obn = osbornite, Ssi = sassite-like mineral and Tta = tistarite.
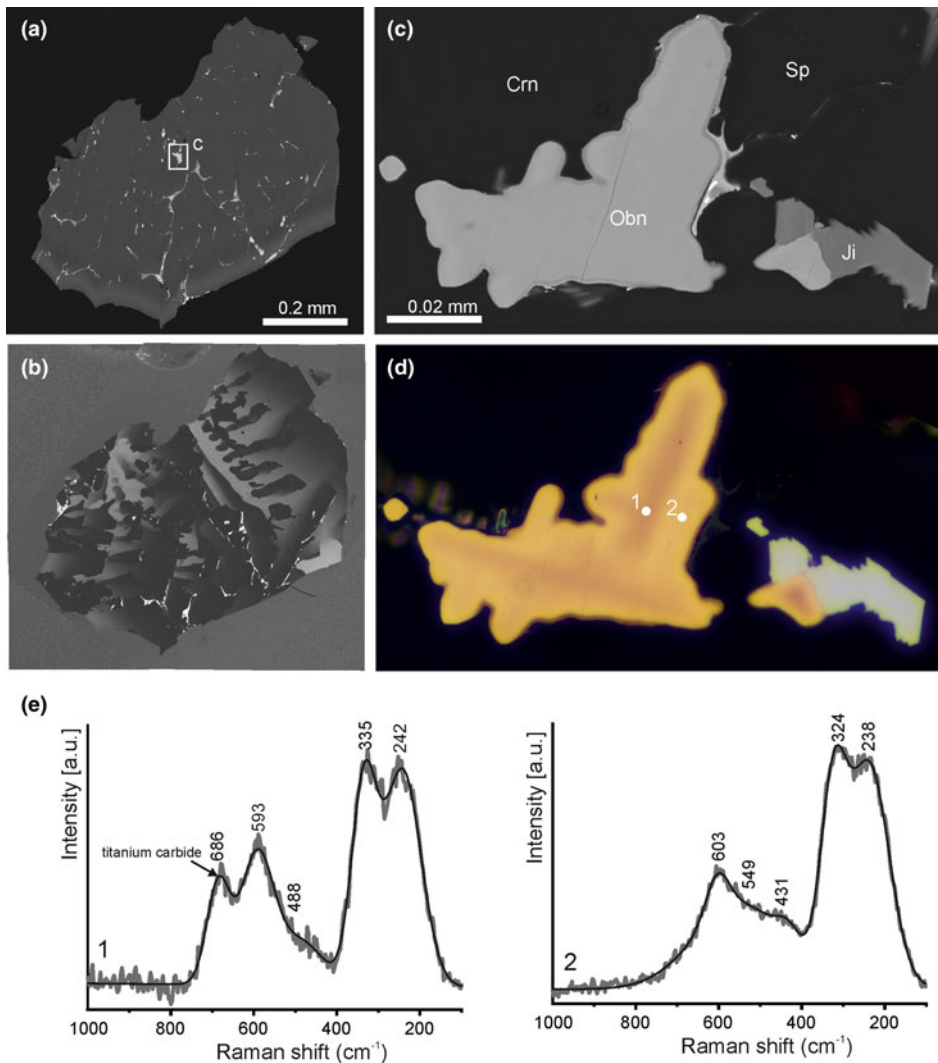
Figure 3. (a,b) Carmel sapphire grain with inclusions of skeletal osbornite crystals: (a) backscattered electron (BSE) image, fragment magnified in (c) and (d) is shown in the frame; and (b) cathodoluminescence, growing inhomogeneity of corundum is visible. (c,d) Cross-section perpendicular to the skeletal crystal elongation of osbornite: (c) BSE image; and (d) reflected light image showing points 1 and 2 for Raman analysis. The central part of the skeletal crystal enriched in C has a darker, brownish colour in (d). (e) Raman spectra for osbornite from location 1; and (f) Raman spectra for osbornite from location 2 marked in (d). Crn = corundum, Ji = jingsuiite, Obn = osbornite and Sp = spinel.
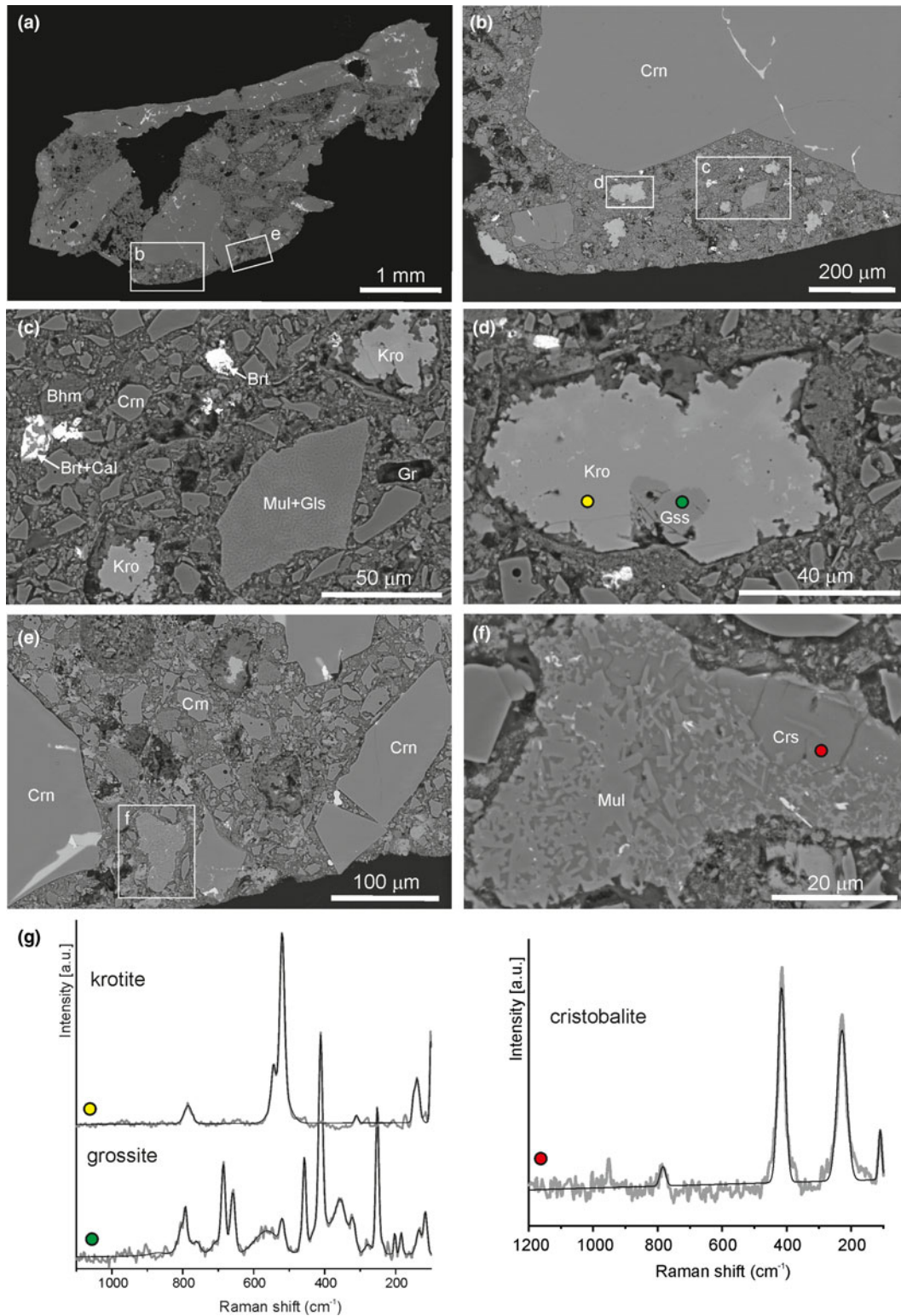
Figure 4. (a–f) BSE images. (a) Typical view of 'white breccia' fragments, with the location of magnified images (b) and (e) marked. (b) Fragment of breccia with krotite and mullite debris in glass, frames are shown for areas magnified in (c) and (d). (c) Glass angular grain with mullite symplectites. (d) Krotite grain with grossite inclusion, points of Raman spectra measurements are shown by yellow (krotite) and green (grossite) circles. (e) Fragment of 'white breccia', with area magnified in (f) indicated. (f) Cristobalite grain with mullite inclusions and red spot indicating the point of Raman spectrum measurement. (g) Raman spectra of minerals marked in (d) and (f). Bhm = böhmite-like mineral, Brt = baryte, Cal = calcite, Crs = cristobalite, Gr = graphite, Gls = glass, Crn = corundum, Gss = grossite, Kro = krotite and Mul = mullite.
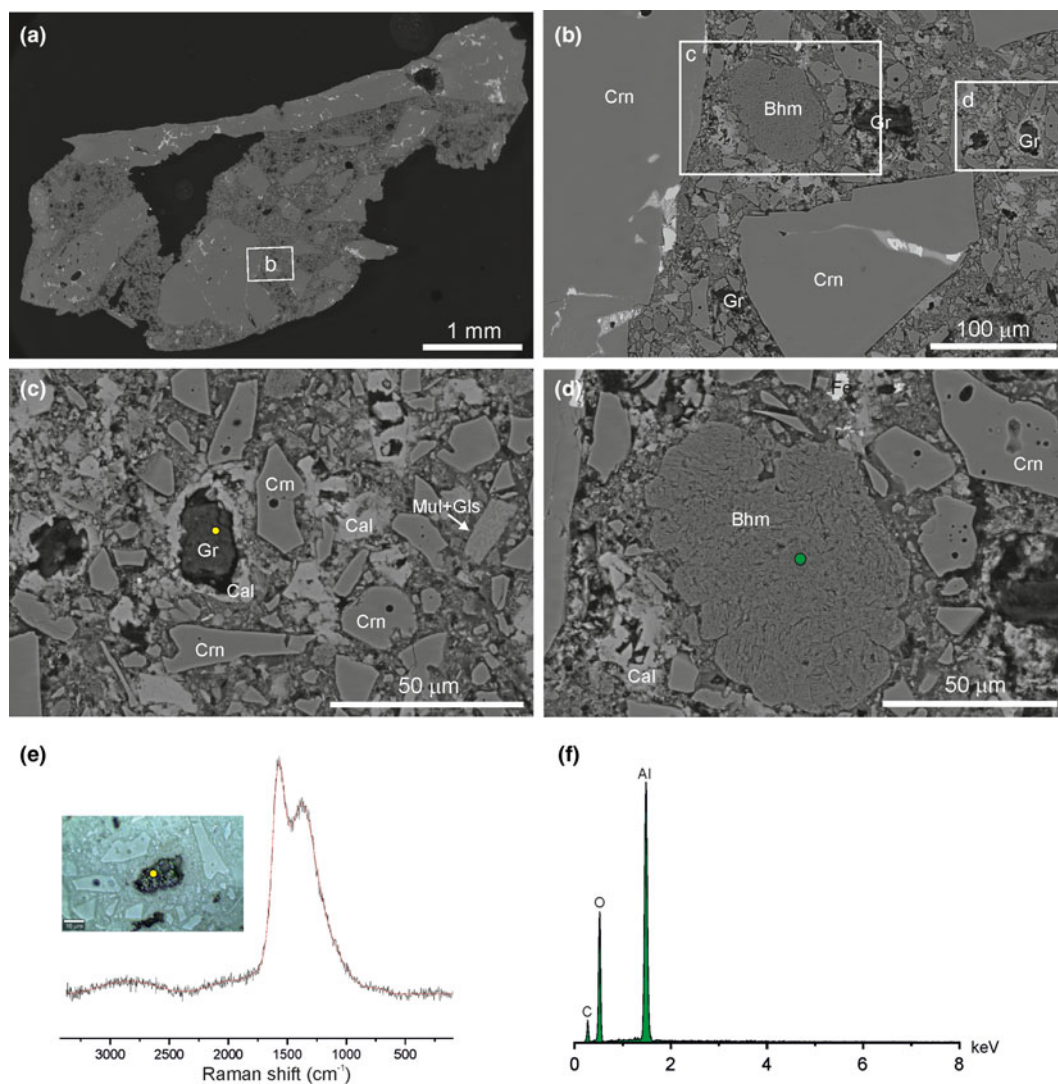
Figure 5. Böhmite-like and graphite-like phases in 'white breccia'. (a) General view of mounted specimen, fragment magnified in (b) is shown in the frame. (b) Breccia fragment enriched in grains of graphite-like substance, areas magnified in (c) and (d) are outlined by frames. (c) Graphite-like grain with calcite rim; yellow spot location of Ramana spectrum measurement. (d) Böhmite-like mineral; green spot shows a place of EDS spectrum measurement. (e) Raman spectrum of graphite-like mineral and its image in the reflected light. (f) EDS spectrum of böhmite-like phase. Bhm = böhmite-like mineral, Cal = calcite, Fe = native iron, Gr = graphite, Gls = glass, Crn = corundum, Mul = mullite.

studied by us and the results of that investigation have been published recently (Galuskin *et al.*, 2022). The mineral is represented by xenomorphic grains that are homogenous in composition (Fig. 2a), and more rarely by crystals with elements of skeletal growth (Fig. 2b). Osbornite is usually associated with schreibersite, barringerite, schreibersite–iron eutectic and native iron (Galuskin *et al.*, 2023). Its composition and structure correspond to stoichiometric TiN (Galuskin *et al.*, 2022).

Osbornite from Carmel sapphire grains forms skeletal crystals, which as a rule are confined to glass inclusions and associated with the super-reduced minerals (Fig. 2c,d; Griffin *et al.*, 2018, 2021b). Griffin *et al.* (2021b) underlines the non-stable composition of osbornite from Carmel sapphire presented by the phases of the TiN–TiC–TiO system, however they do not provide data on the composition trends and zonation of these skeletal crystals. Our investigation of numerous skeletal crystals from Carmel sapphire showed that they exhibit regular zonation:

the centrum of osbornite skeletal crystals is enriched in C, whereas in the rim the N(+O) content increases, as is reflected in the optical properties and well manifested under reflected light (Fig. 3). In the Raman spectra of osbornite from Carmel sapphire, the presence of C impurity (>1–2 wt.%) is displayed in the appearance of a band at 685 cm^{-1} (Fig. 3e; Escobar-Alarcona *et al.*, 2011).

The osbornite inclusions investigated from the synthetic corundum from slags of the fused alumina production (Supplementary Fig. S2) have zonation analogous to the zonation of osbornite from Carmel sapphire: the centrum is enriched in C and the rim in N (+O) (Supplementary Fig. S3).

'White breccia'

A fragment of the 'white breccia' (3×4×7 mm in size, from which a polished mount was prepared) was investigated (Supplementary
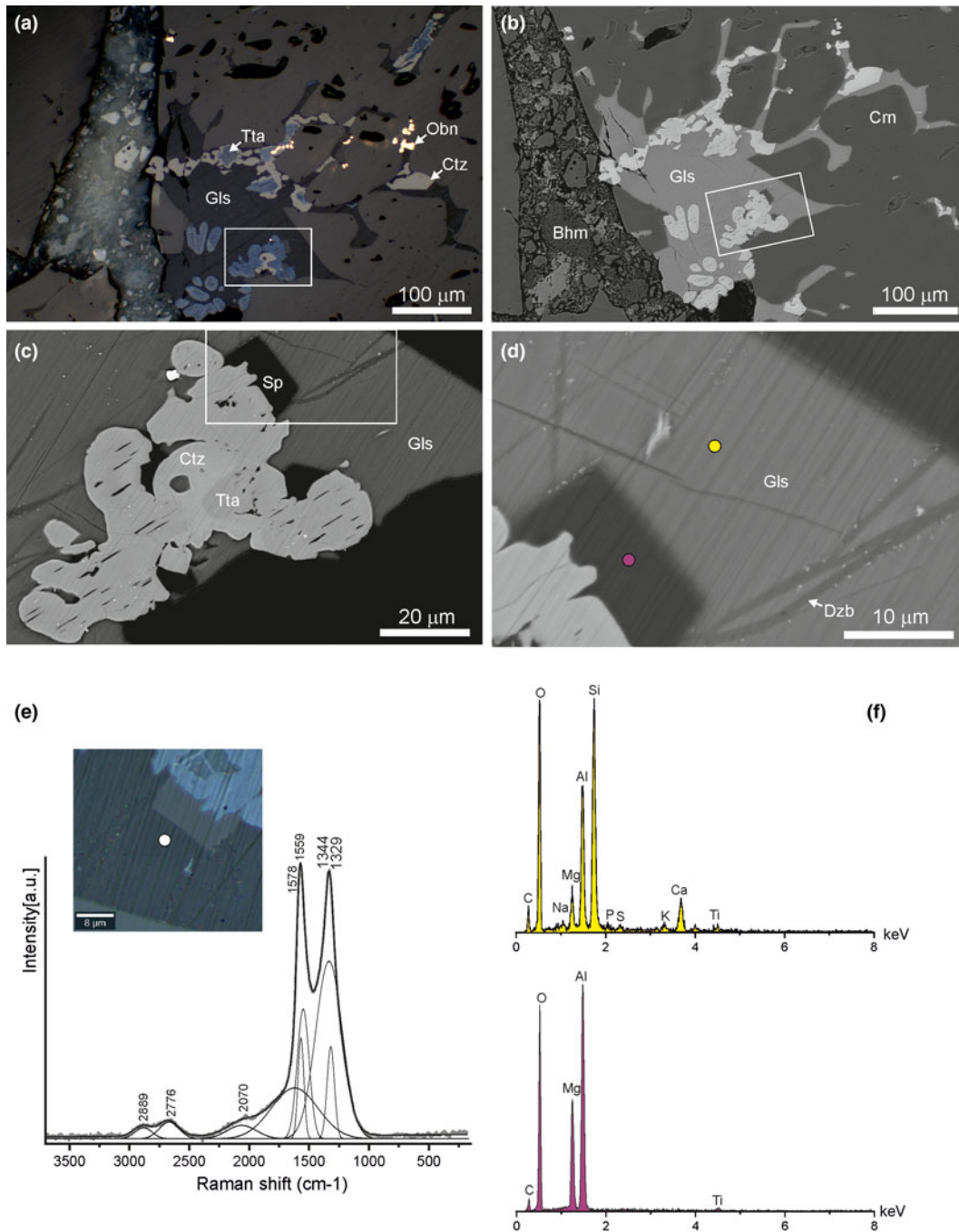
Figure 6. Ti-mineral inclusions in glass of 'white breccia'. (a) Reflected light and (b) BSE images; the fragment magnified in (c) is shown in the frame. (c) Sassite-like mineral, carmeltazite and spinel intergrowth, fragment magnified in (d) is shown in the frame. (d) Glass with striated surface, which appears as a result of re-polishing of the mount with 'white breccia' to a depth of ~0.5 mm. At this depth, the mount sample had only been lightly impregnated with epoxy and so numerous microscopic corundum grains were plucked out and striated the surface of the minerals. Coloured spots show locations of EDS spectra measurement given in (f). (e) Raman spectra of glass with graphite-like phase, inset optical image with white spot shows the place of Raman analysis. (f) EDS spectra of glass (yellow) and spinel (pink). Crn = corundum, Ctz = carmeltazite, Dsb = dmisteinbergite, Gls = glass, Obn = osbornite, Sp = spinel and Tta = tistarite.

Fig. S4). In addition to the blue and light-brown fragments of Carmel sapphire grains and aggregates containing a typical super-reduced mineral association, which has been described several times by Griffin and co-authors (Supplementary Figs S5–S7; Griffin *et al.*, 2016b, 2018, 2019a,b, 2020a,b, 2021a,b), in the white cement we recognise corundum-free fragments 50–200 μm in size. Primarily aggregates of krotite, $CaAl_2O_4$, with grossite, $CaAl_4O_7$, and diaoyudaoite, $NaAl_{11}O_{17}$, inclusions,

and also angular grains presented as mullite in glass or cristobalite (Fig. 4; Supplementary Fig. S8). It should be noted that some Carmel sapphire inclusions in the 'white breccia' intergrowing with dmisteinbergite, $CaAl_2Si_2O_8$, crystals look 'very fresh' and unaltered (Supplementary Fig. S8a).

In the 'white breccia', a rounded porous böhmite-like mineral with 'cauliflower' morphology and graphite-like mineral segregations were identified (Fig. 5).
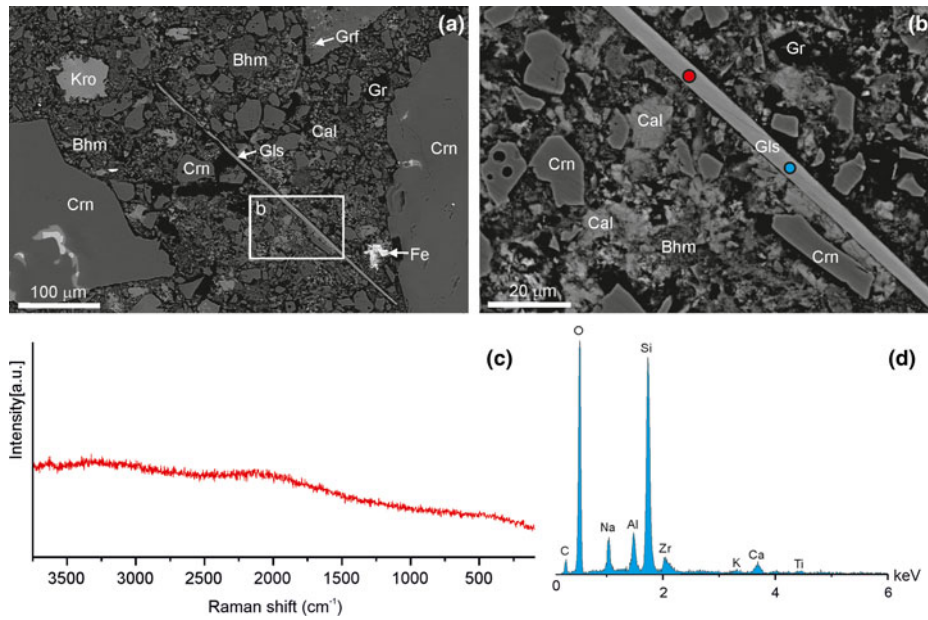
Figure 7. (a) Lamella of Zr-bearing glass in the 'white breccia', fragment magnified in (b) is shown in the frame. (b) The lamella is ∼3 μm in thickness, spots show site of Raman and EDS spectra measurements. (c) Raman spectrum of Zr-bearing glass. (d) EDS spectrum of Zr-bearing glass. Bhm = böhmite-like mineral, Cal = calcite, Gr = graphite, Crn = corundum, Gls = glass, Kro = krotite and Fe = iron.
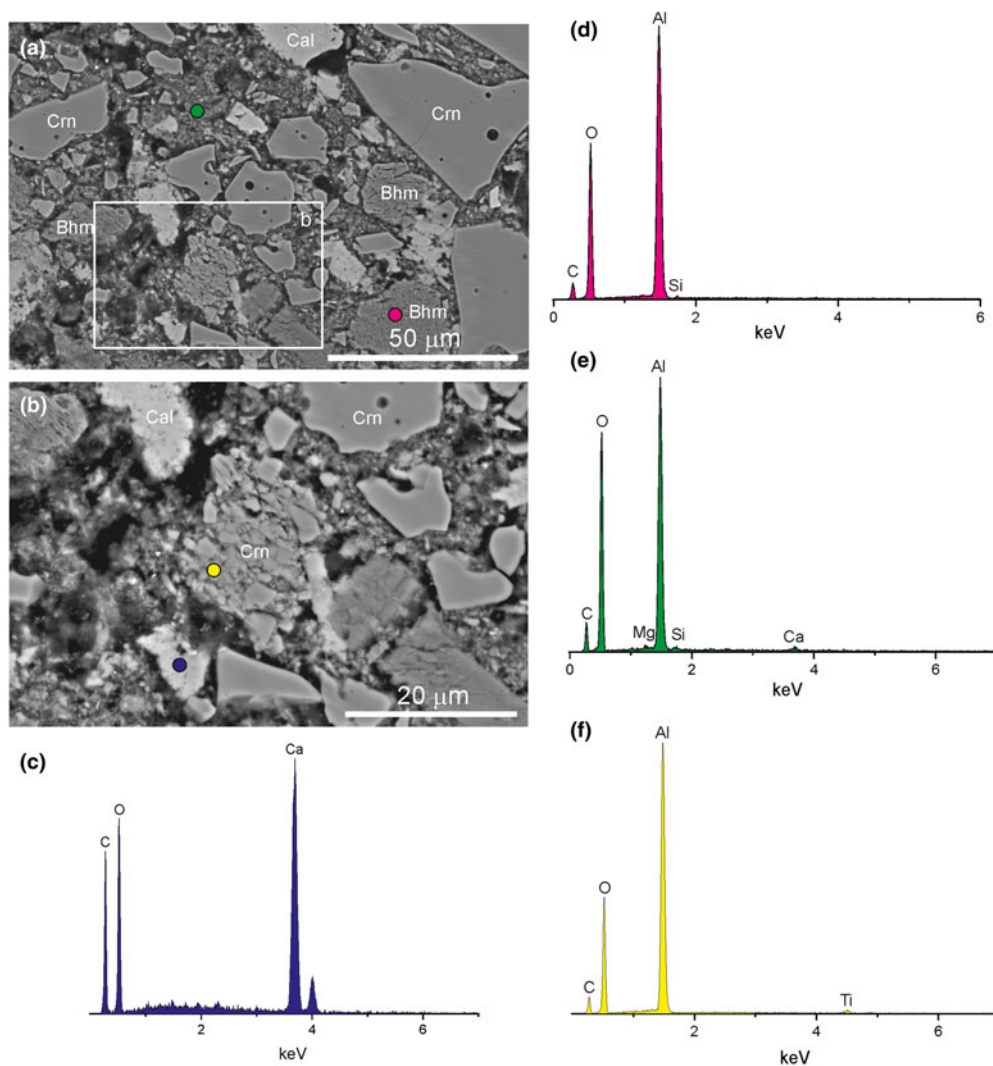
Figure 8. (a) General view of the 'white breccia' fragment, the area magnified in (b) is shown in frame. (b) 'Cracked' corundum grain. Coloured spots show points of EDS analyses. (c–f) EDS spectra: (c) calcite; (d) böhmite-like mineral; (e) cement; and (f) corundum. Bhm = böhmite-like mineral, Cal = calcite and Crn = corundum.

A graphite-like substance in the form of a thin emulsion is also present as inclusions in glass from Carmel sapphire. It is practically invisible in optical or electron microscopes, however in the Raman spectra of the glass, characteristic bands of disordered graphite-like substance appear (Fig. 6).

An occurrence of a Zr-bearing glass lamella, 2–3 μm in thickness, after re-polishing was unexpected (Fig. 7). It is not probable that this thin, brittle glass lamella was added to the mount during repeated grinding on diamond powder; rather, the lamella was in the 'white breccia' cement originally.

As noted above, the predominant type of debris in the investigated 'white breccia' is corundum. Larger corundum aggregates contain silica glass that is typical for the Carmel sapphire inclusion of super-reduced minerals (Supplementary Figs S5–S7). Silica melt is usually squeezed out between corundum grains (Xiong et al., 2017; Fig. 3a), whereas in the corundum ball-like voids (gaseous) are observed (Fig. 5c, 7b). The size of the angular fragments of corundum in the investigated

sample of the 'white breccia' varies from 7 mm to 1 μm or less; there is no sorting of grains by size (Fig. 4c,e; 5c; 7a,b; Supplementary Figs S4, S6D, S7B). There are fragments of 'cracked' corundum, which probably underwent a shock thermal effect (Fig. 8).

The cement of the 'white breccia' is mainly represented by Al-hydroxides (bauxite). It is clearly visible in the X-ray maps of this element (Fig. 9) and confirmed by the energy-dispersive spectroscopy (EDS) analytical data (Fig. 8). Calcite distributed in the breccia is very inhomogeneous (Fig. 7b; Supplementary Fig. S8B), as reflected in the X-ray maps of Ca, C and O (Fig. 9), and typically the mineral forms separate grains (Fig. 8a,b; 10a). In calcite grains, relics of krotite are observed, which indicates that most of the calcite formed as a result of the carbonatisation of Ca-aluminates (Fig. 10b). Thus, the 'white breccia' can be ideally presented as angular grains of Carmel sapphire from 1 μm to 7 mm that are not sorted by size and are cemented by bauxite material.
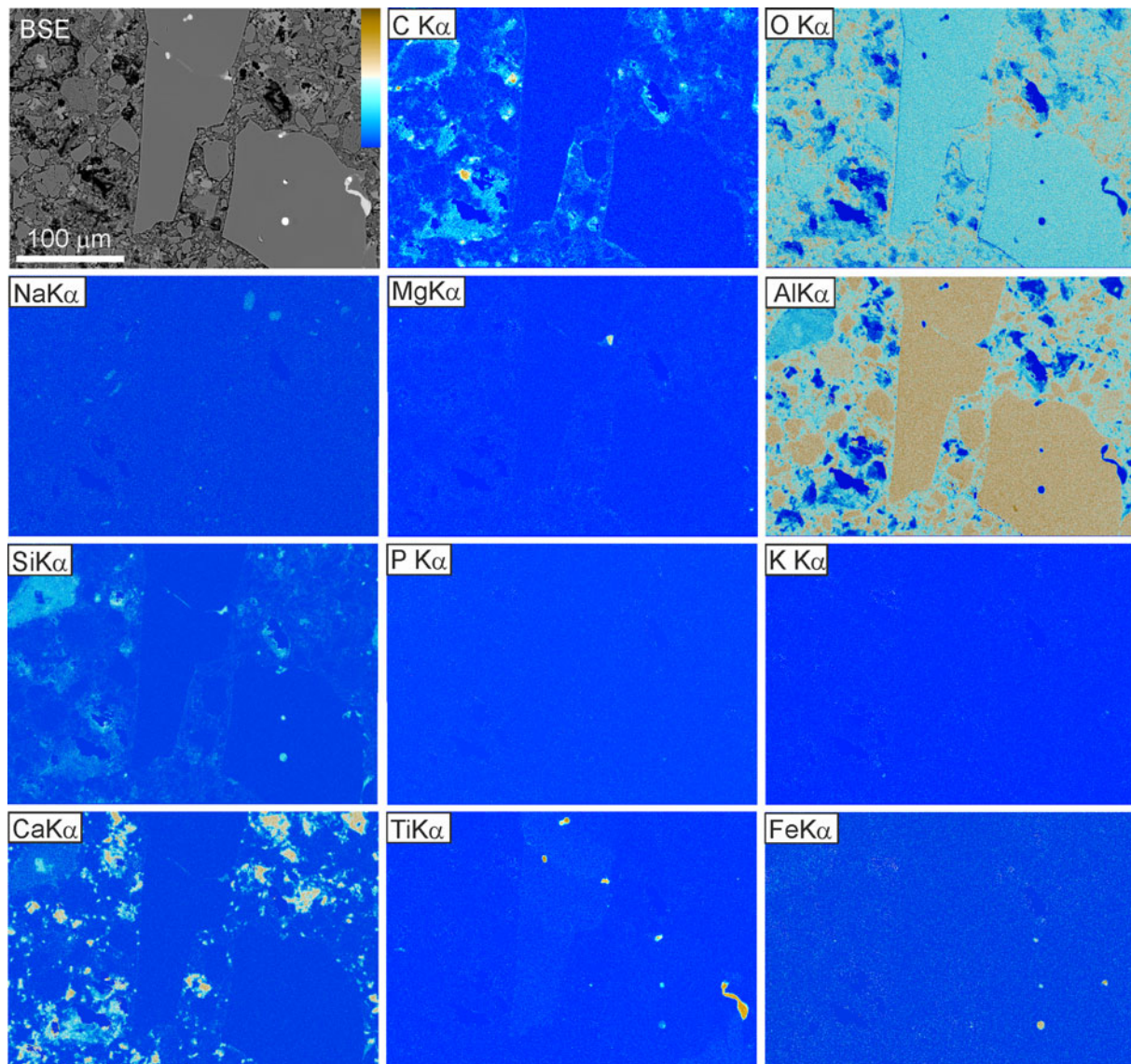
Figure 9. BSE image of 'white breccia'. The colour scale in top right indicates the relative element concentration for the X-ray maps of the chosen elements.
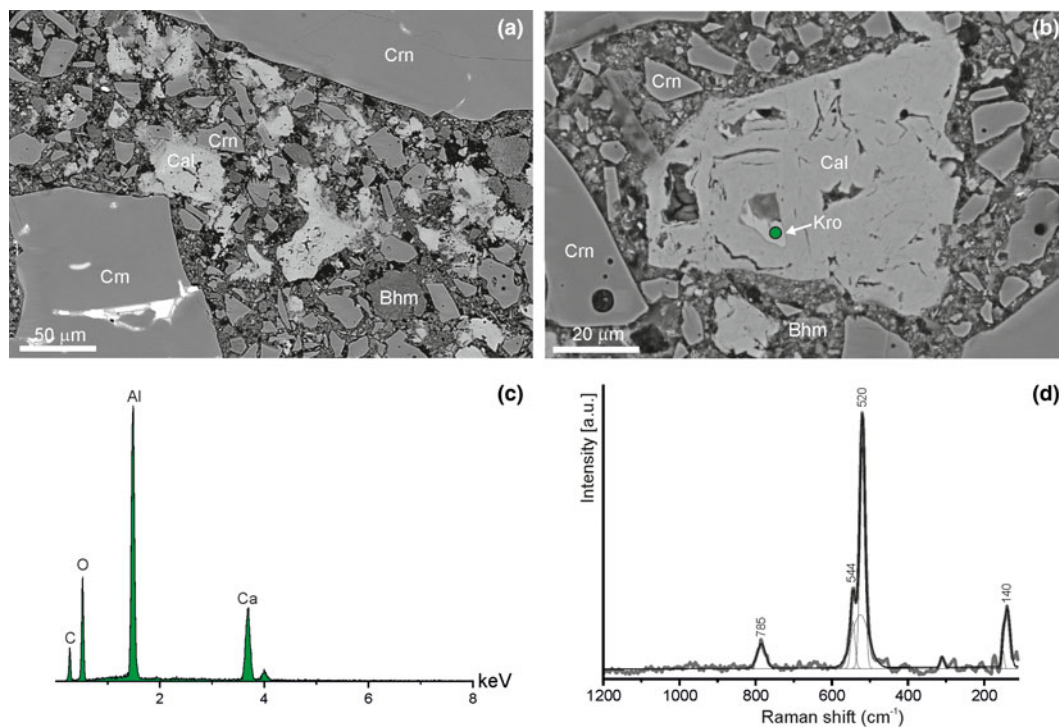
Figure 10. (a) Calcite grains in 'white breccia'. (b) Calcite grain with krotite relics, green spot shows the location of EDS and Raman spectra measurements. (c) EDS and (d) Raman spectrum of krotite. Bhm = böhmite-like mineral, Cal = calcite, Crn = corundum, Kro = krotite.

A comparison of the internal structure of Carmel sapphire and synthetic corundum

For investigation two random grains were selected: (1) pink corundum from a slag sample (Supplementary Fig. S2, Fig. 11a); and (2) light-brown corundum from the 'white breccia' (Fig. 11d). In both grains of corundum there are glass and super-reduced mineral inclusions, which in the back-scattered electron images are distinguished by their lighter colour (Fig. 11b,e). Our investigation shows that aggregates of Carmel sapphire and pink corundum have similar growth inhomogeneity, as is clearly visible in the CL images (Fig. 11c,f).

Discussion

The composition and morphology of inclusions in the corundum from the Mt Carmel 'white breccia' (Supplementary Figs S5–S7) correspond well to the super-reduced minerals in the Carmel sapphire described by Griffin *et al.* (2016b, 2018, 2019a,b, 2020a,b, 2021a,b). The photos of 'white breccia', mentioned by Griffin *et al.* (2019b) as a source of Carmel sapphire, are publicly available (https://www.mining.com/new-mineral-found-inside-gemstones, May 2023 – see Supplementary Fig. S9). We consider that the samples studied of the 'white breccia' from Carmel are identical to those containing Carmel sapphire.

The anthropogenic genesis of Carmel sapphire was proposed by Litasov *et al.* (2019a) on the basis of comparison of super-reduced inclusions in Carmel sapphire with inclusions in fused alumina. Ballhaus *et al.* (2021), with reference to the thermodynamic analysis, have shown that super-reduced phases from Carmel sapphire cannot be stable in the conditions of the mantle–crustal boundary, where, in the opinion of Griffin and co-authors, Carmel sapphire was formed (Griffin *et al.*, 2019a, 2020a). Ballhaus *et al.* (2021), following Litasov *et al.* (2019a),

conclude that Carmel sapphire has an anthropogenic origin. We agree with these authors and provide additional evidence below, which confirms that Carmel sapphire has an anthropogenic origin.

(1) The 'white breccia' is composed of unsorted angular corundum grains and aggregates from 1 μm to 7 mm in size (Fig. 4c,e; 5c; 7a,b; Supplementary Figs S4, S6D, S7B). The debris are cemented by bauxite-like material (Al-hydroxides), which also forms aggregates with 'cauliflower' morphology up to 200 μm in size – characteristic of calcined bauxite (Fig. 5d). Calcite does not represent the breccia cement, and commonly occurs as separated grains, which contain relics of the high-temperature aluminate: krotite (Fig. 10). Thus the 'white breccia' is not a 'carbonate-cemented volcanic ash' and it could not form in marine conditions as is suggested by Griffin *et al.* (2019b). We think that the Carmel sapphire grains were cemented by calcined bauxite used as a component of the furnace mixture for fused alumina production. The 'white breccia' is therefore comprised of the mixed waste of fused alumina production with the material of the furnace mixture. The discovery of Zr-bearing glass used in the production of special laboratory glassware confirms that the 'white breccia' is a mixed waste.

(2) Phases typical for slags of fused alumina production and metallurgical slags were identified in the 'white breccia' (Erokhin *et al.*, 2017; Litasov *et al.*, 2019a). Krotite fragments, commonly with grossite and diaoyudaoite inclusions, are distributed in breccia irregularly (Fig. 4b,c; 7a). Krotite and grossite were discovered and described from meteorites (Weber and Bischoff, 1994; Ma *et al.*, 2011), and terrestrial examples are questionable and require verification. For example, the mineral described by Shulamite Gross with the formula $CaAl_4O_7$ from a pyrometamorphic rock of the Hatrurim Complex is not grossite, as follows from Gross's original description (Gross, 1977). This mineral was identified only by three lines of the diffraction pattern and is
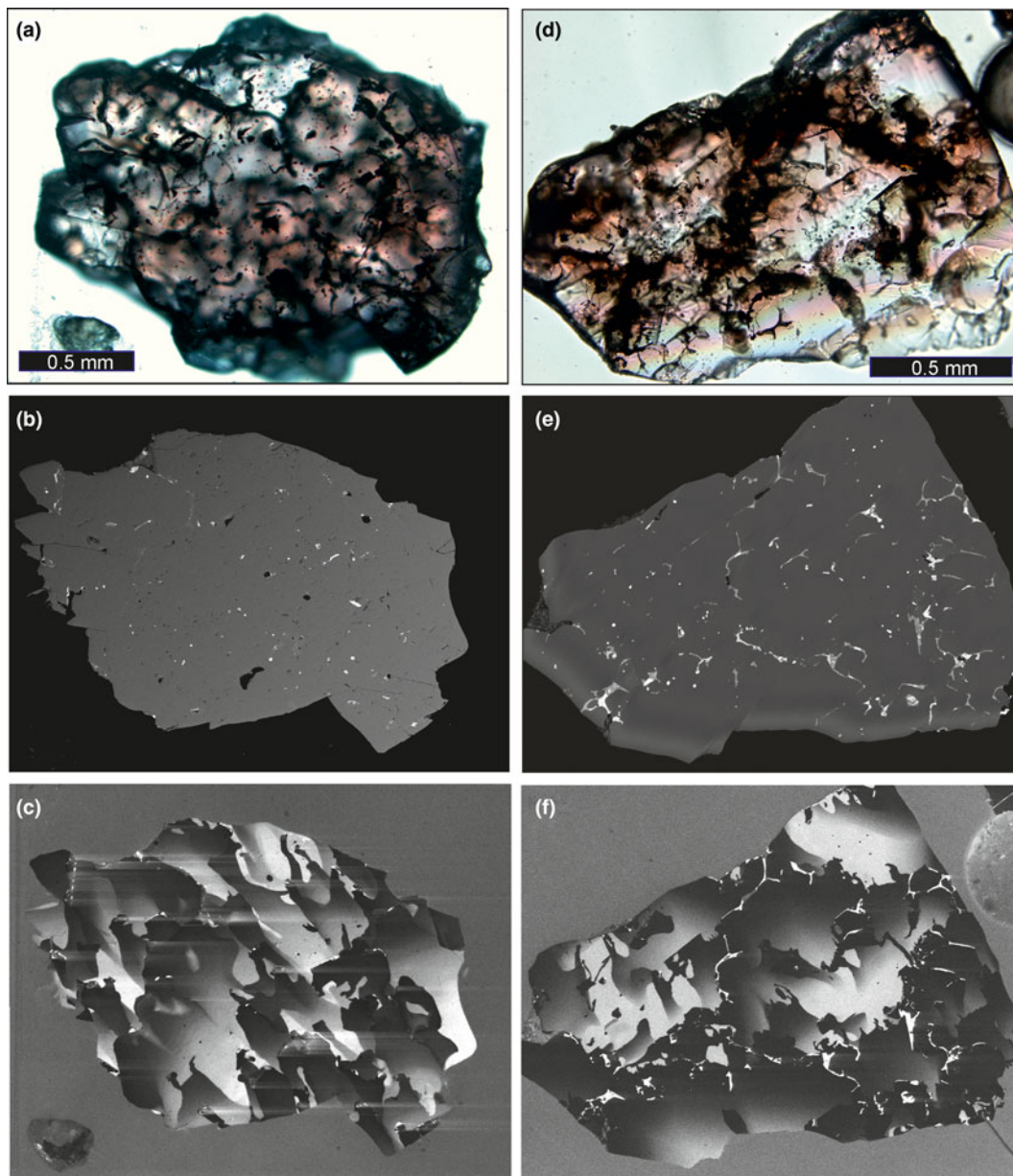
Figure 11. Comparison of growth inhomogeneity of grain aggregates of synthetic corundum (a–c) and Carmel sapphire (d–f). (a, d) – optical images; (b, e) – BSE images; (c, f) – CL images.

characterised by low birefringence, whereas krotite has high birefringence, $\delta = 0.027$. Most likely, it was a product of the hydration of ye'elimite $(Ca_4Al_6(SO_4)O_{12})$ or brownmillerite $(Ca_2AlFe^{3+}O_5)$.

Glass fragments with inclusions of mullite crystals are typical for slags from fused alumina production (Hemberger *et al.*, 2009). We found such fragments with mullite in the 'white breccia' (Fig. 4c,f; Supplementary Fig. S8). It was not surprising to find grains in the 'white breccia' from Carmel sapphire inclusions of a graphite-like material which forms both separated aggregates and an emulsion in silicate glass. We consider that the graphite-like material is the remains of thermally modified coal coke added to the furnace mixture to reduce Fe and Si.

(3) In meteorites and in breccia of the Hatrurim Complex, osbornite associates with iron phosphides and silicates (Bannister, 1941; Weisberg *et al.*, 1988; Galuskin *et al.*, 2022, 2023). There is no mechanism for the simultaneous removal of

Fe and Si from natural melt systems. In the technological process of fused alumina production at temperatures >2000°C there is an almost complete removal of Si and Fe in the form of a melt, which has a lower melting point than corundum, and is gravitationally accumulated in the lower part of the electric furnace in the form of a slag. Very small droplets of the Si–Fe melt remain suspended in the corundum melt and are captured during its crystallisation. Carmel sapphire usually has numerous tiny spherical inclusions of the Si–Fe (±Ti, Cr, Mn…) alloy (Supplementary Fig. S5A), indicating that the removal of Si and Fe occurred at temperatures >2000°C, which is unrealistic for natural magma.

(4) In natural objects (meteorites and pyrometamorphic breccia), osbornite does not form skeletal forms (Fig. 2a,b; Bannister, 1941; Weisberg *et al.*, 1988; Galuskin *et al.*, 2022), whose formation from the melt requires extremely rapid quenching of the melt/fluid. Natural osbornite is represented by grains and crystals

of homogeneous composition, whereas osbornite from Carmel sapphire, which forms skeletal forms, has a chemical zonation characteristic of fused alumina osbornite with enrichment of central zones in carbon (Fig. 3; Supplementary Fig. S3B, D). Also, in Carmel sapphire an overgrowth of the early-forming khamrabaevite, TiC, by osbornite is observed (Supplementary Fig. S6D; Xiong *et al.*, 2017). TiC has a higher melting point than TiN, which determines the sequence of crystallisation: titanium carbide → titanium nitride with decreasing temperature of the corundum melt.

(5) A very similar type of growth heterogeneity (zonal-sectoral structure) of Carmel sapphire and synthetic 'electrocorundum' (Fig. 11) indicates that the crystallisation of the corundum melt proceeded according to a similar scenario in both cases.

In conclusion, our investigation of the 'white breccia', osbornite and associated minerals allow us to conclude unambiguously an anthropogenic origin of Carmel sapphire. Therefore, all new minerals previously described in Carmel sapphire should be discredited by the IMA–CNMNC as they do not meet the basic criterion of a mineral which has a natural origin.

Supplementary material. The supplementary material for this article can be found at https://doi.org/10.1180/mgm.2023.25

Competing interests. The authors declare none.

References

Ballhaus C., Helmy H.M., Fonseca R.O.C., Wirth R., Schreiber A. and Jöns N. (2021) Ultra-reduced phases in ophiolites cannot come from Earth's mantle. *American Mineralogist*, **106**, 1053–1063.

Bannister F.A. (1941) Osbornite, meteoritic titanium nitride. *Mineralogical Magazine*, **26**, 36–44.

Bindi L., Cámara F., Griffin W.L., Huang J.-X., Gain S.E.M., Toledo V. and O'Reilly SY (2019) Discovery of the first natural hydride. *American Mineralogist*, **104**, 611–614.

Bindi L., Cámara F., Gain S.E.M., Griffin W.L., Huang J.-X., Saunders M. and Toledo V. (2020) Kishonite, VH_2, and Oreillyite, Cr_2N, two new minerals from the corundum xenocrysts of Mt Carmel, Northern Israel. *Minerals*, **10**, 1118.

Cámara F., Bindi L., Pagano A., Pagano R., Gain S.E.M. and Griffin W.L. (2019) Dellagiustaite: a novel natural spinel containing V^{2+}. *Minerals*, **9**, 4.

Dobrzhinetskaya L.F., Wirth W., Yang J., Hutcheon I.D., Weber P.K. and Green H.W. (2009) High-pressure highly reduced nitrides and oxides from chromitite of a Tibetan ophiolite. *Proceedings of the National Academy of Sciences USA*, **106**, 19233–19238.

Dobrzhinetskaya L., Mukhin P., Wang Q., Wirth R., O'Bannon E., Zhao W., Eppelbaum L. and Sokhonchuk T. (2018) Moissanite (SiC) with metal-silicide and silicon inclusions from tuff of Israel: Raman spectroscopy and electron microscope studies. *Lithos*, **310–311**, 355–368.

Escobar-Alarcon L., Medina V., Romero E.C.S., Fernandez M. and Solis-Casados D. (2011) Microstructural characterization of Ti–C–N thin films prepared by reactive crossed beam pulsed laser deposition. *Applied Surface Science*, **257**, 9033–9037.

Galuskin E., Galuskina I.O., Kamenetsky V., Vapnik Ye., Kusz J. and Zieliński G. (2022) First *in-situ* terrestrial osbornite (TiN) in the pyrometamorphic Hatrurim Complex, Israel. *Lithosphere*, **2022**, 81277447.

Galuskin E.V., Kusz J., Galuskina I.O., Książek M., Vapnik Ye. and Zieliński G. (2023) Discovery of terrestrial andreyivanovite, FeCrP, and the effect of Cr

and V substitution in barringerite-allabogdanite low-pressure transition. *American Mineralogist*, doi: 10.2138/am-2022-8647

Griffin W.L., Gain S.E.M., Adams D.T., Huang J.-X., Saunders M., Toledo V., Pearson N.J. and O'Reilly S.Y. (2016a) First terrestrial occurrence of tistarite (Ti_2O_3): Ultra-low oxygen fugacity in the upper mantle beneath Mount Carmel, Israel. *Geology*, **44**, 1–4.

Griffin W.L., Gain S.E.M., Adams D.T., Toledo V., Pearson N.J. and O'Reilly S.Y. (2016b) Deep-Earth methane and mantle dynamics: insights from Northern Israel, Southern Tibet and Kamachatka. *Journal and Proceedings of the Royal Society of New South Wales*, **149**, 17–33.

Griffin W.L., Gain S.E.M., Bindi L., Toledo V., Cámara F., Saunders M. and O'Reilly S.Y. (2018) Carmeltazite, $ZrAl_2Ti_4O_{11}$, a new mineral trapped in corundum from volcanic rocks of Mt Carmel, Northern Israel. *Minerals*, **8**, 601.

Griffin W.L., Gain S.E.M., Huang J.-X., Saunders M., Shaw S., Toledo V. and O'Reilly S.Y. (2019a) A terrestrial magmatic hibonite-grossite-vanadium assemblage: desilication and extreme reduction in a volcanic plumbing system, Mount Carmel, Israel. *American Mineralogist*, **104**, 207–219.

Griffin W.L., Toledo V. and O'Reilly S.Y. (2019b) Discussion of "Enigmatic super-reduced phases in corundum from natural rocks: Possible contamination from artificial abrasive materials or metallurgical slags" by Litasov et al. (Lithos, v.340–341, p.181–190). *Lithos*, **348–349**, 191–122.

Griffin W.L., Gaina S.E.M., Cámara F., Bindi L., Shaw J., Alard O., Saunders M., Huang J.-X, Toledo V. and O'Reilly S.Y. (2020a) Extreme reduction: mantle-derived oxide xenoliths from a hydrogen-rich environment. *Lithos*, **358–359**, 1–8.

Griffin W.L., Gain S.E.M., Saunders M., Bindi L., Alard O., Toledo V. and O'Reilly S.Y. (2020b) Parageneses of TiB_2 in corundum xenoliths from Mt. Carmel, Israel: siderophile behavior of boron under reducing conditions. *American Mineralogist*, **105**, 1609–1621.

Griffin W.L., Gain S.E.M., Saunders M., Alard O., Shaw J., Toledo V. and O'Reilly S.Y. (2021a) Nitrogen under super-reducing conditions: Ti oxynitride melts in xenolithic corundum aggregates from Mt Carmel (N. Israel). *Minerals*, **11**, 780.

Griffin W.L., Gain S.E.M., Saunders M., Cámara F., Bindi L., Spartà D., Toledo V. and O'Reilly S.Y. (2021b) Cr_2O_3 in corundum: ultrahigh contents under reducing conditions. *American Mineralogist*, **106**, 1420–1437.

Griffin W.L., Gain S.E.M., Saunders M.J., Huang J.-X., Alard O., Toledo V. and O'Reilly S.Y. (2022) Immiscible metallic melts in the upper mantle beneath Mount Carmel, Israel: silicides, phosphides, and carbides. *American Mineralogist*, **107**, 532–549.

Grokhovsky V.I. (2006) Osbornite in Cb/Ch-like carbonaceous chondrite Isheyevo. 69th Annual Meteoritical Society Meeting, 2006, 52312006.

Gross S. (1977) *The Mineralogy of the Hatrurim Formation, Israel.* Geological Survey of Israel, Jerusalem, Israel, 80 pp.

Hemberger Y., Presser V., Zimmermann J., Krause O. and Nickel K.G. (2009) *Cathodoluminescence microscopy: A fast, powerful method to analyze refractories.* Conference Paper, 52th International Feuerfestkolloquium / International Colloquium on Refractories, Aachen, Germany.

Huang J.-X., Xiong Q., Gain S.E.M., Griffin W.L., Murphy T.D., Shiryaev A.A., Li L., Toledo V., Tomshin M.D. and O'Reilly S.Y. (2020) Immiscible metallic melts in the deep Earth: clues from moissanite (SiC) in volcanic rocks. *Science Bulletin*, **65**, 1479–1488.

Leitner J., Vollmer C. and Hoppe P. (2018) A study of osbornite from enstatite chondrites at the submicrometer scale. 49th Lunar and Planetary Science Conference, LPI Contrib. No. 2083.

Litasov K.D., Kagi H. and Bekker T.B. (2019a) Enigmatic super-reduced phases in corundum from natural rocks: possible contamination from artificial abrasive materials or metallurgical slags. *Lithos*, **340–341**, 181–190.

Litasov K.D., Bekker T.B. and Kagi H. (2019b) Reply to the discussion of "Enigmatic super-reduced phases in corundum from natural rocks: Possible contamination from artificial abrasive materials or metallurgical slags" by Litasov et al. (Lithos, v.340–341, p.181–190) by W.L. Griffin, V. Toledo and S.Y. O'Reilly). *Lithos*, **348–349**, 105170.

Lu J.-G., Griffin W.L., Huang J.-X., Hong-Kun Dai H.-K., Castillo-Oliver M. and O'Reilly S.Y. (2022) Structure and composition of the lithosphere beneath Mount Carmel, North Israel. *Contributions to Mineralogy and Petrology*, **177**, 29.

Ma C., Kampf A.R., Connolly H.C., Beckett J.R., Rossman G.R., Sweeney Smith S.A. and Schrader D.L. (2011) Krotite, $CaAl_2O_4$, a new refractory mineral from the NWA 1934 meteorite. *American Mineralogist*, **96**, 709–715.

Ma C., Bindi L., Cámara F. and Toledo V. (2022a) Griffinite, IMA 2021-110, in: CNMNC Newsletter 66. *Mineralogical Magazine*, **86**, 359–362.

Ma C., Griffin W.L., Bindi L., Cámara F. and Toledo V. (2022b) Magnéliite, IMA 2021-111, in: CNMNC Newsletter 66. *Mineralogical Magazine*, **86**, 359–362.

Ma C., Griffin W.L., Bindi L., Cámara F. and Toledo V (2022c): Ziroite, IMA 2022-013, in: CNMNC Newsletter 68. *Mineralogical Magazine*, **86**, 854–859.

Ma C., Griffin W.L., Bindi L., Cámara F. and Toledo V. (2022d): Sassite, IMA 2022-014, in: CNMNC Newsletter 68. *Mineralogical Magazine*, **86**, 854–859.

Ma C., Griffin W.L., Bindi L., Cámara F. and Toledo V. (2022e): Mizraite-(Ce), IMA 2022-027, in: CNMNC Newsletter 68. *Mineralogical Magazine*, **86**, 854–859.

Ma C., Griffin W.L., Bindi L. and Cámara F. (2022f): Toledoite, IMA 2022-036, in: CNMNC Newsletter 68. *Mineralogical Magazine*, **86**, 854–859.

Ma C., Griffin W.L., Bindi L., Cámara F. and Toledo V. (2023) Yeite, IMA 2022-079, in: CNMNC Newsletter 70. *Mineralogical Magazine*, **87**, 160–168.

Oliveira B., Griffin W.L., Gain S.E.M., Saunders M., Shaw J., Toledo V., Afonso J.C. and O'Reilly S.Y. (2021) Ti^{3+} in corundum traces crystal growth in a highly reduced magma. *Scientific Reports*, **11**, 2439.

Silaev V.I., Karpov G.A., Anikin N.P., Vergasova L.P., Fillipov V.N. and Tarasov K.V. (2019) Mineral-phase paragenesis in explosive products of modern volcanic eruptions in Kamchatka and Kurily. Part 2. Minerals-satellites of diamonds of the Tolbachik type. *Journal Volcanology Seismology*, **6**, 36–49.

Stan C.S., O'Bannon III E.F., Mukhin P., Tamura N. and Dobrzhinetskaya L. (2020) X-ray Laue microdifraction and Raman spectroscopic investigation of natural silicon and moissanite. *Minerals*, **10**, 204.

Tatarintsev V.I., Sandomirskaya S.M. and Tsumbal S.N. (1987) First discovery of titanium nitride (osbornite) in terrestrial rocks. *Proceedings of the USSR Academy of Sciences*, **296**, 1458–1461.

Weber D. and Bischoff A. (1994) Grossite ($CaAl_4O_7$) – a rare phase in terrestrial rocks and meteorites. *European Journal Mineralogy*, **6**, 591–594.

Weisberg M.K., Prinz M. and Nehru C.E. (1988) Petrology of ALH85085 a chondrite with unique characteristics. *Earth and Planetary Science Letters*, **91**, 19–32.

Xiong Q., Griffin W.L., Huang J.-H., Gain S.E.M., Toledo V., Pearson N.J. and O'Reilly S.Y. (2017) Super-reduced mineral assemblages in "ophiolitic" chromitites and peridotites: the view from Mount Carmel. *European Journal Mineralogy*, **29**, 557–570.

Xiong F., Xu X., Mugnaioli E., Gemmi M., Wirth R., Grew E. and Robinson P.T. (2020) Two new minerals, badengzhuite, TiP, and zhiqinite, $TiSi_2$, from the Cr-11 chromitite orebody, Luobusa ophiolite, Tibet, China: is this evidence for super-reduced mantle-derived fluids? *European Journal Mineralogy*, **32**, 557–574.

Xiong F., Xu X., Mugnaioli E., Gemmi M., Wirth R., Grew E.S. and Robinson P.T. (2022) Jingsuiite, TiB_2, a new mineral from the Cr-11 podiform chromitite orebody, Luobusa ophiolite, Tibet, China: Implications for recycling of boron. *American Mineralogist*, **107**, 43–53.

Xu X., Yang J., Guo G. and Xiong F. (2013) Mineral inclusions in corundum from chromitites in the Kangjinla chromite deposit. Tibet. *Acta Petrolei Sinica*, **29**, 1867–1877.

Yatsenko I.G., Skublov S.G., Levashova E.V., Galankina O.L. and Bekesha S.N. (2020) Composition of spherules and lower mantle minerals, isotopic and geochemical characteristics of zircon from volcaniclastic facies of the Mriya lamproite pipe. *Journal of Mining Institute*, **242**, 150–159.

Yatsenko I.G., Galankina O.L., Marin Yu.B. and Skublovb S.G. (2021) Corundum with inclusions of extremely reduced minerals from explosive rocks of the Ukrainian Shield. *Proceedings Russian Academy of Sciences*, **500**, 833–837.

Erokhin Yu., Khiller V.V. and Zakharova L.A. (2017) Cosmic mineralogy in metallurgical slags of the Urals. *Mineralogy of Technogenesis*, **2017**, 72–81.